CRISP: Curriculum based Sequential neural decoders for Polar code family

S. Ashwin Hebbar [†1]   **Viraj Nadkarni** [†1]   **Ashok Vardhan Makkuva** [2]   **Suma Bhat** [1]   **Sewoong Oh** [3]
Pramod Viswanath [1]

Abstract

Polar codes are widely used state-of-the-art codes for reliable communication that have recently been included in the 5th generation wireless standards (5G). However, there remains room for the design of polar decoders that are both efficient and reliable in the short blocklength regime. Motivated by recent successes of data-driven channel decoders, we introduce a novel **CurRI**culum based **S**equential neural decoder for **P**olar codes (CRISP)[*]. We design a principled curriculum, guided by information-theoretic insights, to train CRISP and show that it outperforms the successive-cancellation (SC) decoder and attains near-optimal reliability performance on the Polar$(32, 16)$ and Polar$(64, 22)$ codes. The choice of the proposed curriculum is critical in achieving the accuracy gains of CRISP, as we show by comparing against other curricula. More notably, CRISP can be readily extended to Polarization-Adjusted-Convolutional (PAC) codes, where existing SC decoders are significantly less reliable. To the best of our knowledge, CRISP constructs the first data-driven decoder for PAC codes and attains near-optimal performance on the PAC$(32, 16)$ code.

1. Introduction

Error-correcting codes (codes) are the backbone of modern digital communication. Codes, composed of (encoder, decoder) pairs, ensure reliable data transmission even under noisy conditions. Since the groundbreaking work of (Shannon, 1948), several landmark codes have been proposed: Convolutional codes, low-density parity-check (LDPC) codes, Turbo codes, Polar codes, and more recently, Polarization-Adjusted-Convolutional (PAC) codes (Richardson & Urbanke, 2008). In particular, polar codes, introduced by (Arıkan, 2009), are widely used in practice owing to their reliable performance in the short blocklength regime. A family of variants of polar codes known as PAC codes further improves performance, nearly achieving the fundamental lower bound on the performance of any code at finite lengths, albeit at a higher decoding complexity (Arıkan, 2019). In this paper, we focus on the *decoding* of these two classes of codes, jointly termed the "Polar code family".
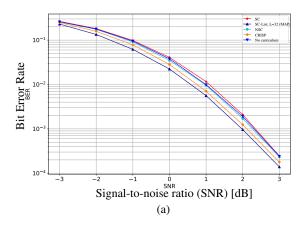
The polar family exhibits several crucial information-theoretic properties; practical finite-length performance, however, depends on high complexity decoders. This search for the design of efficient and reliable decoders for the Polar family is the focus of substantial research in the past decade. **(a) Polar codes:** The classical successive cancellation (SC) decoder achieves information-theoretic capacity asymptotically, but performs poorly at finite blocklengths compared to the optimal maximum a posteriori (MAP) decoder (Arıkan, 2019). To improve upon the reliability of SC, several polar decoders have been proposed in the literature (Sec. 6). One such notable result is the celebrated Successive-Cancellation-with-List (SCL) decoder (Tal & Vardy, 2015). SCL improves upon the reliability of SC and approaches that of the MAP with increasing list size (and complexity). **(b) PAC codes:** The sequential "Fano decoder" (Fano, 1963) allows PAC codes to perform information-theoretically near-optimally; however, the decoding time is long and variable (Rowshan et al., 2020a). Although SC is efficient, $O(n \log n)$, its performance with PAC codes is significantly worse than that of the Fano decoder. Several works (Yao et al., 2021; Rowshan et al., 2020b; Zhu et al., 2020; Rowshan & Viterbo, 2021b;a; Sun et al., 2021) propose ameliorations; it is safe to say that constructing efficient and reliable decoders for the Polar family is an active area of research and of utmost practical interest given the advent of Polar codes in 5G wireless cellular standards. The design of efficient and reliable decoders for the Polar family is the focus of this paper.

In this paper, we introduce a novel **CurRI**culum based

[†]Equal contribution
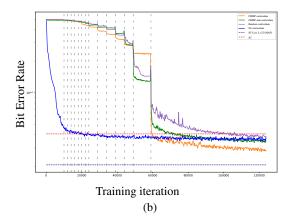[*]Source code available at the following link.

Figure 1: (a) CRISP achieves near-MAP reliability for Polar$(64, 22)$ code on the AWGN channel. (b) Our proposed curriculum is crucial for the gains CRISP attains over the baselines; details in Sec. 4.

Sequential neural decoder for **P**olar code family (CRISP). When the proposed curriculum is applied to neural network decoder training, thus trained decoders outperform existing baselines and attain near-MAP reliabilty on Polar$(64, 22)$, Polar$(32, 16)$ and PAC$(32, 16)$ codes while maintaining low computational complexity (Figs. 1, 5, Table 1). CRISP builds upon an inherent nested hierarchy of polar codes; a Polar(n, k) code subsumes all the codewords of lower-rate subcodes Polar$(n, i), 1 \leq i \leq k$ (Sec. 2.2). We provide principled curriculum of training on examples from a sequence of sub-codes along this hierarchy, and demonstrate that the proposed curriculum is critical in attaining near-optimal performance (Sec. 4).

Curriculum-learning (CL) is a training strategy to train machine learning models, starting with easier subtasks and then gradually increasing the difficulty of the tasks (Wang et al., 2021). (Elman, 1993), a seminal work, was one of the first to employ CL for supervised tasks, highlighting the importance of "starting small". Later, (Bengio et al., 2009) formalized the notion of CL and studied when and why CL helps in the context of visual and language learning (Wu et al., 2020; Wang et al., 2021). In recent years, many empirical studies have shown that CL improves generalization and convergence rate of various models in domains such as computer vision (Pentina et al., 2015; Guo et al., 2018; Wang et al., 2019), natural language processing (Cirik et al., 2016; Platanios et al., 2019), speech processing (Amodei et al., 2016; Gao et al., 2016), generative modeling (Karras et al., 2017; Wang et al., 2018), and neural program generation (Zaremba & Sutskever, 2014; Reed & De Freitas, 2015). Viewed from this context, our results add decoding of algebraic codes (of the Polar family) to the domain of successes of supervised CL. In summary, we make the following contributions:

- We introduce CRISP, a novel curriculum-based sequential neural decoder for the Polar code family. Guided by information-theoretic insights, we propose CL-based techniques to train CRISP, that are crucial for its superior performance (Sec. 3).

- CRISP attains near-optimal reliability performance on Polar$(64, 22)$ and Polar$(32, 16)$ codes whilst achieving improved throughput (Sec. 4.1 and Sec. 4.2).

- CRISP further achieves near-MAP reliability for the PAC$(32, 16)$ code with significantly higher throughput compared to the Fano decoder. To the best of our knowledge, this is the first learning-based PAC decoder to achieve this performance (Sec. 4.5).

2. Problem formulation

In this section we formally define the channel decoding problem and provide background on the Polar code family. Our notation is the following: we denote Euclidean vectors by small bold face letters $\boldsymbol{x}, \boldsymbol{y}$, etc. $[n] \triangleq \{1, 2, \ldots, n\}$. For $\boldsymbol{m} \in \mathbb{R}^n$, $\boldsymbol{m}_{<i} \triangleq (m_1, \ldots, m_{i-1})$. $\mathcal{N}(0, \boldsymbol{I}_n)$ denotes a standard Gaussian distribution in $\mathbb{R}^n$. $\boldsymbol{u} \oplus \boldsymbol{v}$ denotes the bitwise XOR of two binary vectors $\boldsymbol{u}, \boldsymbol{v} \in \{0, 1\}^\ell$.

2.1. Channel decoding

The primary goal of channel decoding is to design efficient decoders that can correctly recover the message bits upon receiving codewords corrupted by noise (Fig. 2). More precisely, let $\boldsymbol{u} = (u_1, \ldots, u_k) \in \{0, 1\}^k$ denote a block of *information/message* bits that we wish to transmit. An encoder $g : \{0, 1\}^k \to \{0, 1\}^n$ maps these message bits into a binary codeword $\boldsymbol{x}$ of length n, i.e. $\boldsymbol{x} = g(\boldsymbol{u})$. The
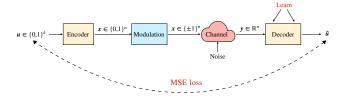
Figure 2: Channel decoding problem.

encoded bits $\boldsymbol{x}$ are modulated via Binary Phase Shift Keying (BPSK), i.e. $\boldsymbol{x} \mapsto 1 - 2\boldsymbol{x} \in \{\pm 1\}^n$, and are transmitted across the channel. We denote both the modulated and unmodulated codewords as $\boldsymbol{x}$. The channel, denoted as $P_{Y|X}(\cdot|\cdot)$, corrupts the codeword $\boldsymbol{x}$ to its noisy version $\boldsymbol{y} \in \mathbb{R}^n$. Upon receiving the corrupted codeword, the decoder f_θ estimates the message bits as $\hat{\boldsymbol{u}} = f_\theta(\boldsymbol{y})$. The performance of the decoder is measured using standard error metrics such as Bit-Error-Rate (BER) or Block-Error-Rate (BLER): $\mathrm{BER}(f_\theta) \triangleq (1/k) \sum_i \mathbb{P}[\hat{\boldsymbol{u}}_i \neq \boldsymbol{u}_i]$, whereas $\mathrm{BLER}(f_\theta) \triangleq \mathbb{P}[\hat{\boldsymbol{u}} \neq \boldsymbol{u}]$.

Given an encoder g with code parameters (n, k) and a channel $P_{Y|X}$, the channel decoding problem can be mathematically formulated as:

$$\theta \in \arg\min_\theta \mathrm{BER}(f_\theta), \tag{1}$$

which is a joint classification of k binary classes. To train the parameters θ, we use the mean-square-error (MSE) loss as a differentiable surrogate to the objective in Eq. 1. It is well known in the literature that naively parametrizing f_θ by general-purpose neural networks does not work well and they perform poorly even for small blocklengths like $n = 16$ (Gruber et al., 2017). Hence it is essential to use efficient decoding architectures that capitalize on the structure of the encoder g (Kim et al., 2018b; Chen & Ye, 2021). To this end, we focus on a popular class of codes, the *Polar code family*, that comprises two state-of-the-art codes: Polar codes (Arıkan, 2009) and Polarization-Adjusted-Convolutional (PAC) codes (Arıkan, 2019). Both these codes are closely related and hence we first focus on polar codes in Sec. 2.2. In Sec. 3, we present CRISP, our novel curriculum-learning based neural decoder to decode polar codes. In Sec. 4.5 we detail PAC codes.

2.2. Polar codes

Encoding. Polar codes, introduced in (Arıkan, 2009), were the first codes to be theoretically proven to achieve capacity for any binary-input discrete memoryless channel. Their encoding is defined as follows: let (n, k) be the code parameters with $n = 2^p, 1 \le k \le n$. In order to encode a block of message bits $\boldsymbol{u} = (u_1, \dots, u_k) \in \{0, 1\}^k$, we first embed them into a source message vector $\boldsymbol{m} \triangleq (m_1, \dots, m_n) = (0, \dots, u_1, 0, \dots, u_2, 0, \dots, u_k, 0, \dots) \in \{0, 1\}^n$, where

$\boldsymbol{m}_{I_k} = \boldsymbol{u}$ and $\boldsymbol{m}_{I_k^C} = 0$ for some $I_k \subseteq [n]$. Since the message block $\boldsymbol{m}$ contains the information bits $\boldsymbol{u}$ only at the indices pertaining to I_k, the set I_k is called the *information set*, and its complement I_k^C the *frozen set*. For the set I_k, we first compute the capacities of the n individual polar bit channels and rank them in their increasing order (Tal & Vardy, 2013). Then I_k picks the top k out of them. For example, $\mathrm{Polar}(4, 2)$ has the ordering $m_1 < m_2 = m_3 < m_4$ and $I_k = \{2, 4\}$, and thus $\boldsymbol{m} = (0, m_2, 0, m_4)$. Similarly, $\mathrm{Polar}(8, 4)$ has $m_1 < m_2 < m_3 < m_5 < m_4 < m_6 < m_7 < m_8$, $I_4 = \{4, 6, 7, 8\}$ and $\boldsymbol{m} = (0, 0, 0, m_4, 0, m_6, m_7, m_8)$.

Finally, we obtain the polar codeword $\boldsymbol{x} = \mathrm{PlotkinTree}(\boldsymbol{m})$, where the mapping $\mathrm{PlotkinTree} : \{0, 1\}^n \to \{0, 1\}^n$ is given by a complete binary tree, known as Plotkin tree (Plotkin, 1960). Fig. 3(a) details the Plotkin tree for $\mathrm{Polar}(4, 2)$. Plotkin tree takes the input message block $\boldsymbol{m} \in \{0, 1\}^n$ at the leaves and applies the "Plotkin" function at each of its internal nodes recursively to obtain the codeword $\boldsymbol{x} \in \{0, 1\}^n$ at the root. The function $\mathrm{Plotkin} : \{0, 1\}^\ell \times \{0, 1\}^\ell \to \{0, 1\}^{2\ell}, \ell \in \mathbb{N}$, is defined as

$$\mathrm{Plotkin}(\boldsymbol{u}, \boldsymbol{v}) \triangleq (\boldsymbol{u} \oplus \boldsymbol{v}, \boldsymbol{v}).$$

For example, in Fig. 3(a), starting with the message block $\boldsymbol{m} = (0, m_2, 0, m_4)$ at the leaves, we first obtain $\boldsymbol{u} = \mathrm{Plotkin}(0, m_2) = (m_2, m_2)$ and $\boldsymbol{v} = \mathrm{Plotkin}(0, m_4) = (m_4, m_4)$. Applying the function once more, we obtain the codeword $\boldsymbol{x} = \mathrm{Plotkin}(\boldsymbol{u}, \boldsymbol{v}) = (m_2 \oplus m_4, m_2 \oplus m_4, m_4, m_4)$.

Decoding. The successive-cancellation (SC) algorithm is one of the most efficient decoders for polar codes, with a decoding complexity of $O(n \log n)$. The basic principle behind the SC algorithm is to sequentially decode one message bit m_i at a time according to the conditional log-likelihood ratio (LLR), $L_i \triangleq \log(\mathbb{P}[m_i = 0|\boldsymbol{y}, \hat{\boldsymbol{m}}_{<i}]/\mathbb{P}[m_i = 1|\boldsymbol{y}, \hat{\boldsymbol{m}}_{<i}])$, given the corrupted codeword $\boldsymbol{y}$ and previous decoded bits $\hat{\boldsymbol{m}}_{<i}$ for $i \in I_k$. Fig. 3(b) illustrates this for the $\mathrm{Polar}(4, 2)$ code: for both the message bits m_2 and m_4, we compute these conditional LLRs and decode them via $\hat{m}_2 = \mathbb{1}\{L_2 < 0\}$ and $\hat{m}_4 = \mathbb{1}\{L_4 < 0\}$. Given the Plotkin tree structure, these LLRs can be efficiently computed sequentially using a depth-first-search based algorithm (App. A).

As discussed in Sec. 1, SC achieves the theoretically optimal performance only asymptotically, and its reliability is sub-optimal at finite blocklengths. SC-list (SCL) decoding improves upon its error-correction performance by maintaining a list of L candidate paths at any time step and choosing the best among them in the end. In fact, for a reasonably large list size L, SCL achieves MAP performance at the cost of increased complexity $O(Ln \log n)$, as highlighted in Table 1.
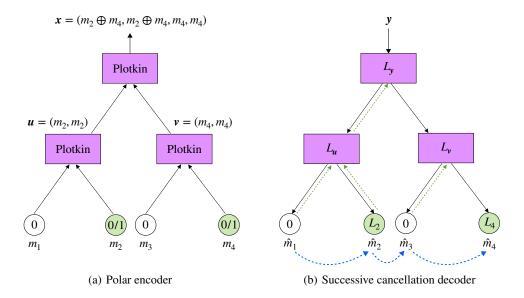
$\boldsymbol{x} = (m_2 \oplus m_4, m_2 \oplus m_4, m_4, m_4)$

(a) Polar encoder

(b) Successive cancellation decoder

Figure 3: Polar$(4, 2)$: (a) Polar encoding via Plotkin tree; (b) Blue arrows indicate the decoding order.

3. CRISP: Curriculum based sequential neural decoder for Polar family

We design CRISP, a curriculum-learning-based sequential neural decoder for polar codes that strictly outperforms the SC algorithm and existing baselines. CRISP uses a sequential RNN decoder, powered by gated recurrent units (GRU) (Cho et al., 2014; Chung et al., 2014), to decode one bit at a time. Instead of standard training techniques, we design a novel curriculum, guided by information-theoretic insights, to train the RNN to learn good decoders. Fig. 4 illustrates our approach.

CRISP decoder. We use the Polar$(4, 2)$ code as a guiding example to illustrate our CRISP decoder (Fig. 4(a)). This code has two message bits (m_2, m_4) and the message block is $\boldsymbol{m} = (0, m_2, 0, m_4)$. Upon encoding it to the polar codeword $\boldsymbol{x} \in \{\pm 1\}^4$ and receiving its noisy version $\boldsymbol{y} \in \mathbb{R}^4$, the decoder estimates the message as $\hat{\boldsymbol{m}} = (0, \hat{m}_2, 0, \hat{m}_4)$. Similar to SC, CRISP uses the sequential paradigm of decoding one bit $\hat{m}_i$ at a time by capitalizing on the previous decoded bits $\hat{\boldsymbol{m}}_{<i}$ and $\boldsymbol{y}$. To that end, we parametrize the bit estimate $\hat{m}_i$ conditioned on the past as a fully connected neural network (FCNN) that takes the hidden state $\boldsymbol{h}_i$ as its input. Here $\boldsymbol{h}_i$ denotes the hidden state of the GRU that implicitly encodes this past information $(\hat{\boldsymbol{m}}_{<i}, \boldsymbol{y})$ via GRU's recurrence equation, i.e.

$$\boldsymbol{h}_i = \text{GRU}_\theta(\boldsymbol{h}_{i-1}, \hat{m}_{i-1}, \boldsymbol{y}), \quad i \in \{1, 2, 3, 4\}, \tag{2}$$

$$\hat{m}_i | \boldsymbol{y}, \hat{\boldsymbol{m}}_{<i} = \text{FCNN}_\theta(\boldsymbol{h}_i), \quad i \in \{2, 4\}, \tag{3}$$

where θ denotes the FCNN and GRU parameters jointly. Henceforth we refer to our decoder as either CRISP or

CRISP$_\theta$. Note that while the RNN is unrolled for $n = 4$ time steps (Eq. 2), we only estimate bits at $k = 2$ information indices, i.e. $\hat{m}_2$ and $\hat{m}_4$ (Eq. 3). A key drawback of SC is that a bit error at a position i can contribute to the future bit errors $(> i)$, and it does not have a feedback mechanism to correct these error events. On the other hand, owing to the RNN's recurrence relation (Eq. 2), through the gradient it receives during training, CRISP can learn to better predict the bits.

Curriculum-training of CRISP. Given the decoding architecture of CRISP in Fig. 4(a), a natural approach to train its parameters via supervised learning is to use a joint MSE loss function for both the bits $(\hat{m}_2, \hat{m}_4)$: $\text{MSE}(\hat{m}_2, \hat{m}_4) = (\hat{m}_2(\theta) - m_2)^2 + (\hat{m}_4(\theta) - m_4)^2$. However, as we highlight in Sec. 4.1 such an approach learns to fail better decoders than SC and gets stuck at local minima. To address this issue, we propose a curriculum-learning based approach to train the RNN parameters.

The key idea behind our curriculum training of CRISP is to decompose the problem of joint estimation of bits $(\hat{m}_2, \hat{m}_4)$ into a sequence of sub-problems with increasing difficulty: start with learning to estimate only the first bit $(\hat{m}_2)$ and progressively add one new message bit at each curriculum step $(\hat{m}_4)$ until we estimate the full message block $\boldsymbol{m} = (\hat{m}_2, \hat{m}_4)$. We freeze all the non-trainable message bits to zero during any curriculum step. In other words, in the first step, we freeze the bit m_4 and train the decoder only to estimate the bit $\hat{m}_2$ (i.e. the subcode corresponding to
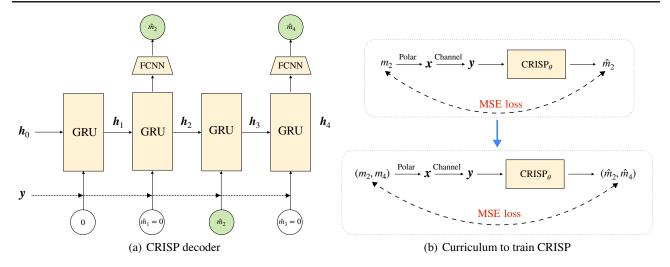
(a) CRISP decoder

(b) Curriculum to train CRISP

Figure 4: CRISP decoder and its training by curriculum-learning for Polar$(2, 4)$.

$k = 1$):

$$(m_2, m_4 = 0) \rightarrow \boldsymbol{m} = (0, m_2, 0, 0) \xrightarrow{\text{Polar}} \boldsymbol{x}$$

$$\boldsymbol{x} \xrightarrow{\text{Channel}} \boldsymbol{y} \xrightarrow{\text{CRISP}_\theta} \hat{m}_2. \qquad (4)$$

We use this trained θ as an initialization for the next task of estimating both the bits $(\hat{m}_2, \hat{m}_4)$:

$$(m_2, m_4) \rightarrow \boldsymbol{m} = (0, m_2, 0, m_4) \xrightarrow{\text{Polar}} \boldsymbol{x}$$

$$\boldsymbol{x} \xrightarrow{\text{Channel}} \boldsymbol{y} \xrightarrow{\text{CRISP}_\theta} (\hat{m}_2, \hat{m}_4). \qquad (5)$$

Fig. 4(b) illustrates this curriculum-learning approach. We note that the knowledge of decoding $\hat{m}_2$ when $m_4 = 0$ (Eq. 4) serves as a good initialization when we learn to decode $\hat{m}_2$ for a general $m_4 \in \{0, 1\}$ (Eq. 5). With such a curriculum aided training, we show in Sec. 4.1 (Figs. 1, 5) that the CRISP decoder outperforms the existing baselines and attains near-optimal performance for a variety of block-lengths and codes. We interpret this in Sec. 4.4. We defer the training details to App. E.

Left-to-Right (L2R) curriculum for Polar(n, k). For a general Polar(n, k) code, we follow a similar curriculum to train CRISP$_\theta$. Denoting the index set by $I_k = \{i_1, i_2, \ldots, i_k\} \subseteq [n]$ in the increasing order of indices $i_1 < i_2 < \ldots < i_k$, our curriculum is given by: Train θ on $\hat{m}_{i_1} \rightarrow$ Train θ on $(\hat{m}_{i_1}, \hat{m}_{i_2}) \rightarrow \ldots \rightarrow$ Train θ on $(\hat{m}_{i_1}, \ldots, \hat{m}_{i_k})$. We term this curriculum *Left-to-Right (L2R)*. The anti-curriculum *R2L* refers to progressively training in the decreasing order of the indices in I_k.
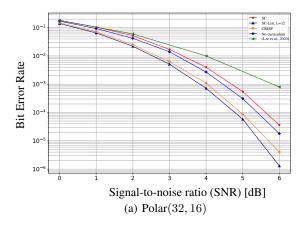
4. Main results

In this section, we present numerical results for the CRISP decoder on the Polar code family.

4.1. AWGN channel

Data generation. The input message $\boldsymbol{u} \in \{0, 1\}^k$ is randomly drawn uniformly from the boolean hypercube and encoded as a polar codeword $\boldsymbol{x} \in \{\pm 1\}^n$. The classical additive white Gaussian noise (AWGN) channel, $\boldsymbol{y} = \boldsymbol{x} + \boldsymbol{z}, \boldsymbol{z} \sim \mathcal{N}(0, \sigma^2 \boldsymbol{I}_n)$, generates the training/test data $(\boldsymbol{y}, \boldsymbol{u})$ for the decoder. The signal-to-noise ratio, i.e. SNR $= -10 \log_{10} \sigma^2$, characterizes the noise level in the channel. Here we fix the channel to be AWGN in all our experiments, as per the standard convention (Kim et al., 2018b), and refer to App. D for additional results on fading and t-distributed channels. App. E details the training procedure. Once trained, we use the CRISP models for comparison against the baselines.

Baselines. The optimal channel decoder is the MAP estimator: $\hat{\boldsymbol{u}} = \arg\max_{\boldsymbol{u} \in \{0,1\}^k} \mathbb{P}[\boldsymbol{u}|\boldsymbol{y}]$, whose complexity grows exponentially in k and is computationally infeasible. Given this, we compare our CRISP decoder with the SCL (Tal & Vardy, 2015), which has near-MAP performance for a large L, along with the classical SC. Among learning-based decoders, we choose the state-of-the-art Neural-Successive-Cancellation (NSC) as our baseline (Doan et al., 2018). NSC replaces sub-components of the existing successive cancellation decoder with NNs to scale decoding to block lengths longer than 32. Each of these neural networks are trained with the LLR outputs of the SC algorithm. Since this training procedure with SC probabilities as the target is sub-optimal, we consider an improved version with end-to-end training (Fig. 2) for a fair comparison. We also include the performance of CRISP trained directly without the curriculum. We also compare with the curriculum training procedure of (Lee et al., 2020) (the original work achieves a reliability worse than SC decoding for block length 32). All these baselines have the same number of parameters as
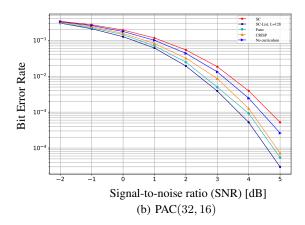
(a) Polar(32, 16)

(b) PAC(32, 16)

Figure 5: CRISP outperforms baselines and attains near-MAP performance for Polar(32, 16) and PAC(32, 16) codes on the AWGN channel.

CRISP.

Results. Fig. 1(a) highlights that the CRISP decoder outperforms the existing baselines and attains near-MAP performance over a wide range of SNRs for the Polar(64, 22) code. Fig. 1(b) illustrates the mechanism behind these gains at 0dB: the curriculum-guided CRISP slowly improves upon the overall BER (over the 22 bits) during the training and eventually achieves much better performance than SC and other baselines. In contrast, the decoder trained from scratch makes a big initial gain but gets stuck at local minima and only achieves a marginal improvement over SC. Moreover, we see that decoders trained using other curricula, e.g. R2L, also fail to show significant improvements over SC (Figs. 1(b), 11). We observe a similar trend for Polar(32, 16) code in Fig. 5(a), where CRISP achieves near-MAP performance. We posit that aided by a good curriculum, CRISP avoids getting stuck at bad local minima and converges to better minima in the optimization landscape. Further, CRISP is robust to deviations from the AWGN channel, while attaining similar performance gains over SC on fading and T-distributed channels (App. D). For additional results, we refer to App. D which highlights similar reliability gains for other blocklengths and rates, App. C for the ablation analysis, and App. E for the training hyperparameters and architectures.

Sequential vs Block decoding. We note that the sequential RNN architecture for CRISP is inspired in part by the sequential SC algorithm. Notwithstanding, we also design block decoders that estimate all the information bits m_i in one shot given $\boldsymbol{y}$. We choose 1D Convolutional Neural Networks (CNNs) to parameterize this block decoder, *CRISP_CNN*. CRISP_CNN, trained with the L2R curriculum, achieves similar BER performance as CRISP

(App. C.2).

4.2. Reliability-throughput comparison

Table 1: Throughput and reliability comparison of various decoders on Polar(n, k).

Decoder	Throughput (in Mbps)				Gap to SCL, L=32 (in dB)	
	(32, 16)		(64, 22)		(32, 16)	(64, 22)
	GPU	CPU	GPU	CPU		
SC	0.17	27	0.08	15	0.80	0.40
FastSC	N/A	**47**	N/A	**40**	0.80	0.40
SCL, L=4	0.01	8.5	0.02	6.27	0.05	0.10
FastSCL, L=4	N/A	**30**	N/A	**24**	0.05	0.10
SCL, L=32 (MAP)	5e-3	0.81	2e-3	0.60	**0.00**	**0.00**
FastSCL, L=32	N/A	7.7	N/A	5.5	0.00	0.00
NSC	N/A	N/A	32.6	0.02	N/A	0.35
CRISP_GRU (Ours)	**80**	0.04	**38.7**	0.02	0.15	**0.20**
CRISP_CNN (Ours)	**250**	0.02	**133**	0.13	0.15	0.20
CRISP_GRU - No curriculum	80	0.04	38.7	0.02	0.60	0.35

In the previous section, we demonstrated that CRISP achieves better reliability than the baselines. Here we analyze these gains through the lens of *decoding complexity*. To quantitatively compare the complexities of these decoders, we evaluate their throughput on a single GTX 1080 Ti GPU as well as a CPU (Intel i7-6850K, 12 threads). For the GPU version, we use our implementation of SC/SCL owing to the lack of publicly available implementations. On the other hand, for the CPU column we use an optimized multithreaded implementation of SC/FastSC, SCL/FastSCL (Léonardon et al., 2019) in C++ by (Cassagne et al., 2019). As Table 1 highlights, CRISP exploits the GPUs' inherent optimization towards NNs to achieve excellent throughput, whilst achieving near-SCL BER performance. We note that CRISP_CNN (App. C.2) attains better throughput than CRISP_GRU, while maintaining gains in BER. We posit that further improvement in throughput can be realized using techniques like pruning and knowledge distillation. This

is beyond the scope of this paper and is an important and separate direction of future research. Note that we use BER$= 10^{-3}$ to compute the gap to SCL (Figs. 1(a), 5(a)). We refer to App. F for further discussion.

4.3. Computational complexity

Running CRISP on suitable hardware architectures allows it to attain significant throughput gains. Nevertheless, to provide a more comprehensive performance evaluation, it's important to also consider other metrics such as power consumption. This necessitates an analysis of the computational complexity of the algorithm, which we present below.

The decoding complexity of SCL is $O(Ln \log n)$, where L represents the list size. On the other hand, CRISP employs a 2-layer GRU neural network, the computational complexity of which is $n(2h(n+1) + 6h^2)$, where h denotes the dimension of the GRU's hidden state. The bulk of this computational complexity involves matrix-vector multiplications; modern hardware like GPUs which allow for significant speedups in these operations. This, in turn, allows for an improved performance and efficiency of CRISP on such platforms.

4.4. Interpretation

This section describes why L2R is a better curriculum than others. To this end, we first claim that learning to decode uncorrupted codewords ($\boldsymbol{y} = \boldsymbol{x}$) is critical to learning a reliable decoder. This claim follows from the following key observation: while training our model (sequential or block) at a specific SNR, we observe that whenever our model reaches SC or better performance, its BER on uncorrupted codewords, aka the noiseless BER, drops to zero very early in the training (App. B, Fig. 7(a)). On the other hand, when the model gets stuck at bad minima even after a lot of training, its noiseless BER is high (Fig. 7(b)). Hence, without loss of generality, we focus on the setting $\boldsymbol{y} = \boldsymbol{x}$. Under this noiseless scenario, we analyze how the optimal bit decoding rules evolve for different curricula. In particular, we focus on the least reliable bits as they contribute the largest to noiseless BER (Fig. 8(a) and Fig. 8(b)).

For the Polar$(4, 4)$ code, Fig. 6(a) illustrates how the optimal rule evolves for its least reliable bit m_1. In this case, the MAP decoding rule for m_1 is: $\hat{m}_1 = x_1 x_2 x_3 x_4$. Under the L2R curriculum, we arrive at this expression via $x_1 \rightarrow x_1 x_2 \rightarrow x_1 x_2 x_3 \rightarrow x_1 x_2 x_3 x_4$, whereas R2L follows $1 \rightarrow 1 \rightarrow 1 \rightarrow x_1 x_2 x_3 x_4$. This highlights that L2R reaches the optimal rule more gracefully by learning to include one coordinate x_i at a time while this change for R2L (and no-curriculum) is abrupt, making it harder to learn. Fig. 9 illustrates a similar evolution for the remaining bits (m_2, m_3, m_4).

More concretely, we define the notion of *learning difficulty* for a bit: the number of bits multiplied in its optimal decoding rule. This metric roughly captures the number of operations a model has to learn at any curriculum step. Fig. 6(b) illustrates how it evolves over the L2R and R2L curricula for the least reliable bit in Polar$(64, 22)$. If we take the maximum learning difficulty over all bits, we obtain a similar plot (Fig. 10). Note that in both the plots, the jumps in learning difficulty are larger for R2L, thus indicating a harder transfer than L2R, where it increases smoothly (at most one bit per step).

4.5. PAC codes

A recent breakthrough work (Arıkan, 2019) introduces a new class of codes called Polarization-Adjusted-Convolutional (PAC) codes that match the fundamental lower bound on the performance of any code under the MAP decoding at finite-lengths (Moradi et al., 2020). The motivating idea behind PAC codes is to overcome two key limitations of polar codes at finite blocklengths: the poor minimum distance properties of the code and the sub-optimality of SC compared to the MAP (Mondelli et al., 2014). This is addressed by adding a *convolutional outer code*, with an appropriate indexing I_k, before polar encoding to improve the distance properties of the resulting code. More formally, the message block $\boldsymbol{u} \in \{0, 1\}^k$ is embedded into the source vector $\boldsymbol{m} \in \{0, 1\}^n$ according to the Reed-Muller (RM) indices $I_k^{(\mathrm{RM})}$: compute the Hamming weights of integers $0, 1, \ldots, n - 1$ and choose the top k. Now we encode the message $\boldsymbol{m}$ via a rate-1 convolutional code, i.e. $\boldsymbol{v} = \boldsymbol{c} * \boldsymbol{m} \in \{0, 1\}^n \Leftrightarrow v_i = \sum_j c_j m_{i-j}$, for some 1D convolutional kernel $\boldsymbol{c} \in \{0, 1\}^\ell$. Finally we obtain the PAC codeword $\boldsymbol{x}$ by polar encoding $\boldsymbol{v}$: $\boldsymbol{x} = \mathrm{PlotkinTree}(\boldsymbol{v})$.

PAC codes can be decoded using the classical Fano algorithm (Fano, 1963), a sequential decoding algorithm that uses backtracking. Coupled with the Fano decoder, PAC codes achieve impressive results outperforming polar codes (with SCL decoder) and matching the finite-length capacity bound (Polyanskiy et al., 2010). However, the Fano decoder has significant drawbacks like variable running time, large time complexity at low-SNRs (Rowshan et al., 2020b), and sensitivity to the choice of hyperparameters (Moradi, 2020). To overcome these issues, several non-learning techniques, such as stack/list decoding, adaptive path metrics, etc., have been proposed in the literature (Yao et al., 2021; Zhu et al., 2020; Rowshan & Viterbo, 2021b;a; Sun et al., 2021). In contrast, we design a curriculum-learning-based CRISP decoder for PAC codes trained directly from the data. We use the same L2R curriculum to decode PAC codes.

Fig. 5(b) highlights that the CRISP decoder achieves near-MAP performance for the PAC$(32, 16)$ code. While Fano decoding achieves similar reliability, it is inherently non-
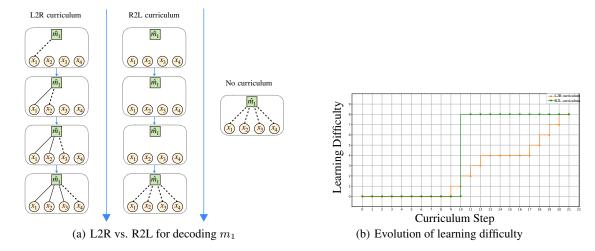
(a) L2R vs. R2L for decoding m_1

(b) Evolution of learning difficulty

Figure 6: L2R vs. R2L: (a) Bit estimates evolve more smoothly under L2R than R2L for Polar$(4, 4)$, (b) Learning difficulty increases more gracefully for L2R than R2L for Polar$(64, 22)$.

parallelizable. In contrast, CRISP allows for batching, and achieves a higher throughput, as highlighted in Table 2. Here we measure the throughput of Fano (Rowshan et al., 2020a) at SNR $= 1$ dB. We note that the existing implementation of Fano is not supported on GPUs. These preliminary results suggest that curriculum-based training holds a great promise for designing efficient PAC decoders, especially for longer blocklengths, which is an interesting topic of future research (App. D.2).

Table 2: Throughput and reliability comparison of various decoders on PAC$(32, 16)$.

Decoder	Throughput (in Mbps)		Gap to SCL, L=128 (in dB)
	GPU	CPU	
SC	N/A	**27**	1.0
SCL, L=128	N/A	0.02	**0.0**
Fano	N/A	4e-3	0.1
CRISP_GRU (Ours)	**80**	0.03	0.4
CRISP_CNN (Ours)	**250**	0.15	0.4
CRISP_GRU - No curriculum	80	0.03	0.8

5. Information theory guided curricula

In Sec. 4, we demonstrated the superiority of L2R curriculum over other schemes. Here we introduce an alternate curriculum, *Noisy-to-Clean (N2C)*, that slightly bests the L2R, inspired by the polarization property of polar codes. The key idea behind N2C curriculum is to capitalize on the polar index set I_k. Recall that the set I_k is obtained by ranking the n polar bit channels (under SC decoding) in the increasing order of their reliabilities (from noisy to clean) and choosing the top k indices. Formally, given $I_k = \{i_{r1}, i_{r2}, \ldots, i_{rk}\} \subseteq [n]$ in the increasing order of reliabilities, our *N2C* curriculum is given by: Train θ on $\hat{m}_{i_{r1}} \rightarrow$ Train θ on $(\hat{m}_{i_{r1}}, \hat{m}_{i_{r2}}) \rightarrow \ldots \rightarrow$ Train θ on

$(\hat{m}_{i_{r1}}, \ldots, \hat{m}_{i_{rk}})$. For both the sequential and block decoders, we observe that N2C is the best curriculum and we have N2C $\approx$ L2R $>$ C2N $\approx$ R2L (Fig. 11). This ordering is consistent with our interpretation in Sec. 4.4 of how the learning difficulty evolves over a curriculum (Fig. 12). For both N2C and L2R, the learning difficulty evolves smoothly but is abrupt for C2N and R2L, thus making transfer harder in these curricula. Note that the *C2N* curriculum refers to progressively training on subcodes of Polar(n, k): Polar$(n, 1) \rightarrow \ldots \rightarrow$ Polar(n, k) (Lee et al., 2020).

6. Related work

To address the sub-optimality of SC at finite lengths, a popular technique is to use list decoding (Tal & Vardy, 2015; Balatsoukas-Stimming et al., 2015), aided by cyclic redundancy checks (CRC) (Li et al., 2012; Niu & Chen, 2012a; Miloslavskaya & Trifonov, 2014). Several alternate decoding methods have also been proposed such as stack decoding (Niu & Chen, 2012b; Trifonov, 2018), belief propagation decoding (Yuan & Parhi, 2014; Elkelesh et al., 2018). Deep learning for communication (Qin et al., 2019; Kim et al., 2020) has been an active field in the recent years and has seen success in many problems including the design of neural decoders for existing linear codes (Nachmani et al., 2016; O'shea & Hoydis, 2017; Lugosch & Gross, 2017; Vasić et al., 2018; Liang et al., 2018; Bennatan et al., 2018; Jiang et al., 2019a; Nachmani & Wolf, 2019; Buchberger et al., 2020; He et al., 2020), and jointly learning channel encoder-decoder pairs. (O'Shea et al., 2016; Kim et al., 2018a; Jiang et al., 2019b; Makkuva et al., 2021; Jamali et al., 2021; Chahine et al., 2021a;b).

Earlier works on designing neural polar decoders (Gross

et al., 2020) used off-the-shelf neural architectures. These were only able to decode codes of small blocklength (≤ 16) (Lyu et al., 2018; Cao et al., 2020). Later works augmented belief propagation decoding (Xu et al., 2018; Doan et al., 2019), with neural components and improved performance. In (Cammerer et al., 2017a) and (Doan et al., 2018), the authors replace sub-components of the existing SC decoder with NNs to scale decoding to longer lengths. However, these methods fail to give reasonable reliability gains compared to SC. In contrast, we use curriculum learning to train neural decoders, and show non-trivial gains over SC performance. (Lee et al., 2020) consider a curriculum training of polar decoder, but do not achieve SC reliability for block length 32. This is owing to the sub-optimality of both the architecture and training curriculum (the C2N scheme). In contrast, we design a principled curriculum guided by information theoretic insights, and a neural architecture that fully capitalizes on the sequential polar decoding. Fig. 11 and Fig. 5(a) show that these design choices are essential for achieving the reliability gains over SC.

Recent research by Choukroun and Wolf (Choukroun & Wolf, 2022b;a) introduces transformer-based neural decoders for block channel codes. A distinctive feature of their approach is the use of a sparse attention mask, which harnesses the structure of the parity check matrix. The application of a similar curriculum training procedure, as used in our work with CRISP, to these transformer-based architectures might potentially expedite the convergence process. Furthermore, such enhancements in the training procedure could potentially close the gap to MAP performance for higher block lengths.

7. Conclusion

We introduce a novel curriculum based neural decoder, CRISP, that attains near-optimal reliability on the Polar code family in the short blocklength regime. We design a principled curriculum to train CRISP, which is crucial to achieve reliability gains for both the Polar and PAC codes. To the best of our knowledge, this is the first learning-based PAC decoder to achieve near-MAP reliability with significantly better throughput than the Fano decoder. Extending our results to medium blocklengths (100-1000) and codes outside the Polar family are interesting future directions. While optimizing the decoder complexity is not the primary focus of this paper, our preliminary results already show gains in throughput over standard methods. Further improvement in decoding complexity whilst maintaining reliability gains is another exciting future research direction.

References

Amodei, D., Ananthanarayanan, S., Anubhai, R., Bai, J., Battenberg, E., Case, C., Casper, J., Catanzaro, B., Cheng, Q., Chen, G., et al. Deep speech 2: End-to-end speech recognition in english and mandarin. In *International conference on machine learning*, pp. 173–182. PMLR, 2016.

Anwar, S., Hwang, K., and Sung, W. Structured pruning of deep convolutional neural networks, 2015. URL https://arxiv.org/abs/1512.08571.

Arikan, E. Channel polarization: A method for constructing capacity-achieving codes for symmetric binary-input memoryless channels. *IEEE Transactions on Information Theory*, 55(7):3051–3073, Jul 2009. ISSN 0018-9448. doi: 10.1109/tit.2009.2021379. URL http://dx.doi.org/10.1109/TIT.2009.2021379.

Arıkan, E. From sequential decoding to channel polarization and back again. *arXiv preprint arXiv:1908.09594*, 2019.

Balatsoukas-Stimming, A., Parizi, M. B., and Burg, A. Llr-based successive cancellation list decoding of polar codes. *IEEE transactions on signal processing*, 63(19):5165–5179, 2015.

Bengio, Y., Louradour, J., Collobert, R., and Weston, J. Curriculum learning. In *Proceedings of the 26th annual international conference on machine learning*, pp. 41–48, 2009.

Bennatan, A., Choukroun, Y., and Kisilev, P. Deep learning for decoding of linear codes-a syndrome-based approach. In *2018 IEEE International Symposium on Information Theory (ISIT)*, pp. 1595–1599. IEEE, 2018.

Brown, T. B., Mann, B., Ryder, N., Subbiah, M., Kaplan, J., Dhariwal, P., Neelakantan, A., Shyam, P., Sastry, G., Askell, A., Agarwal, S., Herbert-Voss, A., Krueger, G., Henighan, T., Child, R., Ramesh, A., Ziegler, D. M., Wu, J., Winter, C., Hesse, C., Chen, M., Sigler, E., Litwin, M., Gray, S., Chess, B., Clark, J., Berner, C., McCandlish, S., Radford, A., Sutskever, I., and Amodei, D. Language models are few-shot learners, 2020. URL https://arxiv.org/abs/2005.14165.

Buchberger, A., Häger, C., Pfister, H. D., Schmalen, L., and Amat, A. G. Pruning neural belief propagation decoders. In *2020 IEEE International Symposium on Information Theory (ISIT)*, pp. 338–342. IEEE, 2020.

Cammerer, S., Gruber, T., Hoydis, J., and Ten Brink, S. Scaling deep learning-based decoding of polar codes via partitioning. In *GLOBECOM 2017-2017 IEEE global communications conference*, pp. 1–6. IEEE, 2017a.

Cammerer, S., Leible, B., Stahl, M., Hoydis, J., and ten Brink, S. Combining belief propagation and successive cancellation list decoding of polar codes on a gpu platform. In *2017 IEEE international conference on acoustics, speech and signal processing (ICASSP)*, pp. 3664–3668. IEEE, 2017b.

Cao, Z., Zhu, H., Zhao, Y., and Li, D. Learning to denoise and decode: A novel residual neural network decoder for polar codes. In *2020 IEEE 92nd Vehicular Technology Conference (VTC2020-Fall)*, pp. 1–6. IEEE, 2020.

Cassagne, A., Hartmann, O., Léonardon, M., He, K., Leroux, C., Tajan, R., Aumage, O., Barthou, D., Tonnellier, T., Pignoly, V., Le Gal, B., and Jégo, C. Aff3ct: A fast forward error correction toolbox! *Elsevier SoftwareX*, 10: 100345, October 2019.

Chahine, K., Jiang, Y., Nuti, P., Kim, H., and Cho, J. Turbo autoencoder with a trainable interleaver. *arXiv preprint arXiv:2111.11410*, 2021a.

Chahine, K., Ye, N., and Kim, H. Deepic: Coding for interference channels via deep learning. *arXiv preprint arXiv:2108.06028*, 2021b.

Chen, X. and Ye, M. Cyclically equivariant neural decoders for cyclic codes. *arXiv preprint arXiv:2105.05540*, 2021.

Cho, K., Van Merriënboer, B., Bahdanau, D., and Bengio, Y. On the properties of neural machine translation: Encoder-decoder approaches. *arXiv preprint arXiv:1409.1259*, 2014.

Choukroun, Y. and Wolf, L. Denoising diffusion error correction codes. *arXiv preprint arXiv:2209.13533*, 2022a.

Choukroun, Y. and Wolf, L. Error correction code transformer. *arXiv preprint arXiv:2203.14966*, 2022b.

Chung, J., Gulcehre, C., Cho, K., and Bengio, Y. Empirical evaluation of gated recurrent neural networks on sequence modeling. *arXiv preprint arXiv:1412.3555*, 2014.

Cirik, V., Hovy, E., and Morency, L.-P. Visualizing and understanding curriculum learning for long short-term memory networks. *arXiv preprint arXiv:1611.06204*, 2016.

Devlin, J., Chang, M.-W., Lee, K., and Toutanova, K. Bert: Pre-training of deep bidirectional transformers for language understanding, 2018. URL https://arxiv.org/abs/1810.04805.

Doan, N., Hashemi, S. A., and Gross, W. J. Neural successive cancellation decoding of polar codes. In *2018 IEEE 19th international workshop on signal processing advances in wireless communications (SPAWC)*, pp. 1–5. IEEE, 2018.

Doan, N., Hashemi, S. A., Mambou, E. N., Tonnellier, T., and Gross, W. J. Neural belief propagation decoding of crc-polar concatenated codes. In *ICC 2019-2019 IEEE International Conference on Communications (ICC)*, pp. 1–6. IEEE, 2019.

Elkelesh, A., Ebada, M., Cammerer, S., and Ten Brink, S. Belief propagation list decoding of polar codes. *IEEE Communications Letters*, 22(8):1536–1539, 2018.

Elman, J. L. Learning and development in neural networks: The importance of starting small. *Cognition*, 48(1):71–99, 1993.

Fano, R. A heuristic discussion of probabilistic decoding. *IEEE Transactions on Information Theory*, 9(2):64–74, 1963.

Gao, T., Du, J., Dai, L.-R., and Lee, C.-H. Snr-based progressive learning of deep neural network for speech enhancement. In *INTERSPEECH*, pp. 3713–3717, 2016.

Gross, W. J., Doan, N., Ngomseu Mambou, E., and Ali Hashemi, S. Deep learning techniques for decoding polar codes. *Machine learning for future wireless communications*, pp. 287–301, 2020.

Gruber, T., Cammerer, S., Hoydis, J., and ten Brink, S. On deep learning-based channel decoding. In *2017 51st Annual Conference on Information Sciences and Systems (CISS)*, pp. 1–6. IEEE, 2017.

Guo, S., Huang, W., Zhang, H., Zhuang, C., Dong, D., Scott, M. R., and Huang, D. Curriculumnet: Weakly supervised learning from large-scale web images. In *Proceedings of the European Conference on Computer Vision (ECCV)*, pp. 135–150, 2018.

Han, X., Liu, R., Liu, Z., and Zhao, L. Successive-cancellation list decoder of polar codes based on gpu. In *2017 3rd IEEE International Conference on Computer and Communications (ICCC)*, pp. 2065–2070. IEEE, 2017.

He, K., Zhang, X., Ren, S., and Sun, J. Deep residual learning for image recognition, 2015. URL https://arxiv.org/abs/1512.03385.

He, Y., Zhang, J., Jin, S., Wen, C.-K., and Li, G. Y. Model-driven dnn decoder for turbo codes: Design, simulation, and experimental results. *IEEE Transactions on Communications*, 68(10):6127–6140, 2020.

Hendrycks, D. and Gimpel, K. Gaussian error linear units (gelus), 2016. URL https://arxiv.org/abs/1606.08415.

Hinton, G., Vinyals, O., and Dean, J. Distilling the knowledge in a neural network, 2015. URL https://arxiv.org/abs/1503.02531.

Hochreiter, S. and Schmidhuber, J. Long short-term memory. *Neural Computation*, 9(8):1735–1780, 1997. doi: 10.1162/neco.1997.9.8.1735.

Jamali, M. V., Saber, H., Hatami, H., and Bae, J. H. Productae: Towards training larger channel codes based on neural product codes. *arXiv preprint arXiv:2110.04466*, 2021.

Jiang, Y., Kannan, S., Kim, H., Oh, S., Asnani, H., and Viswanath, P. Deepturbo: Deep turbo decoder. In *2019 IEEE 20th International Workshop on Signal Processing Advances in Wireless Communications (SPAWC)*, pp. 1–5. IEEE, 2019a.

Jiang, Y., Kim, H., Asnani, H., Kannan, S., Oh, S., and Viswanath, P. Turbo autoencoder: Deep learning based channel codes for point-to-point communication channels. In *Advances in Neural Information Processing Systems*, pp. 2758–2768, 2019b.

Jiao, X., Yin, Y., Shang, L., Jiang, X., Chen, X., Li, L., Wang, F., and Liu, Q. Tinybert: Distilling bert for natural language understanding, 2019. URL https://arxiv.org/abs/1909.10351.

Karras, T., Aila, T., Laine, S., and Lehtinen, J. Progressive growing of gans for improved quality, stability, and variation. *arXiv preprint arXiv:1710.10196*, 2017.

Kim, H., Jiang, Y., Kannan, S., Oh, S., and Viswanath, P. Deepcode: Feedback codes via deep learning. *Advances in neural information processing systems*, 31, 2018a.

Kim, H., Jiang, Y., Rana, R., Kannan, S., Oh, S., and Viswanath, P. Communication algorithms via deep learning. *arXiv preprint arXiv:1805.09317*, 2018b.

Kim, H., Oh, S., and Viswanath, P. Physical layer communication via deep learning. *IEEE Journal on Selected Areas in Information Theory*, 2020.

Lamb, A., Goyal, A., Zhang, Y., Zhang, S., Courville, A., and Bengio, Y. Professor forcing: A new algorithm for training recurrent networks, 2016. URL https://arxiv.org/abs/1610.09038.

Lee, H., Seo, E. Y., Ju, H., and Kim, S.-H. On training neural network decoders of rate compatible polar codes via transfer learning. *Entropy*, 22(5):496, 2020.

Léonardon, M., Cassagne, A., Leroux, C., Jégo, C., Hamelin, L.-P., and Savaria, Y. Fast and flexible software polar list decoders. *Journal of Signal Processing Systems*, 91(8):937–952, 2019.

Li, B., Shen, H., and Tse, D. An adaptive successive cancellation list decoder for polar codes with cyclic redundancy check. *IEEE communications letters*, 16(12):2044–2047, 2012.

Liang, F., Shen, C., and Wu, F. An iterative bp-cnn architecture for channel decoding. *IEEE Journal of Selected Topics in Signal Processing*, 12(1):144–159, 2018.

Loshchilov, I. and Hutter, F. Sgdr: Stochastic gradient descent with warm restarts, 2016. URL https://arxiv.org/abs/1608.03983.

Loshchilov, I. and Hutter, F. Decoupled weight decay regularization. *arXiv preprint arXiv:1711.05101*, 2017.

Lugosch, L. and Gross, W. J. Neural offset min-sum decoding. In *2017 IEEE International Symposium on Information Theory (ISIT)*, pp. 1361–1365. IEEE, 2017.

Lyu, W., Zhang, Z., Jiao, C., Qin, K., and Zhang, H. Performance evaluation of channel decoding with deep neural networks. In *2018 IEEE International Conference on Communications (ICC)*, pp. 1–6. IEEE, 2018.

Makkuva, A. V., Liu, X., Jamali, M. V., Mahdavifar, H., Oh, S., and Viswanath, P. Ko codes: inventing nonlinear encoding and decoding for reliable wireless communication via deep-learning. In *International Conference on Machine Learning*, pp. 7368–7378. PMLR, 2021.

Miloslavskaya, V. and Trifonov, P. Sequential decoding of polar codes. *IEEE Communications Letters*, 18(7):1127–1130, 2014.

Mondelli, M., Hassani, S. H., and Urbanke, R. L. From polar to reed-muller codes: A technique to improve the finite-length performance. *IEEE Transactions on Communications*, 62(9):3084–3091, 2014.

Moradi, M. On the metric and computation of pac codes. *arXiv preprint arXiv:2012.05511*, 2020.

Moradi, M., Mozammel, A., Qin, K., and Arikan, E. Performance and complexity of sequential decoding of pac codes. *arXiv preprint arXiv:2012.04990*, 2020.

Nachmani, E. and Wolf, L. Hyper-graph-network decoders for block codes. *Advances in Neural Information Processing Systems*, 32:2329–2339, 2019.

Nachmani, E., Be'ery, Y., and Burshtein, D. Learning to decode linear codes using deep learning. In *2016 54th Annual Allerton Conference on Communication, Control, and Computing (Allerton)*, pp. 341–346. IEEE, 2016.

Niu, K. and Chen, K. Crc-aided decoding of polar codes. *IEEE communications letters*, 16(10):1668–1671, 2012a.

Niu, K. and Chen, K. Stack decoding of polar codes. *Electronics letters*, 48(12):695–697, 2012b.

O'Shea, T. J., Karra, K., and Clancy, T. C. Learning to communicate: Channel auto-encoders, domain specific regularizers, and attention. In *2016 IEEE International Symposium on Signal Processing and Information Technology (ISSPIT)*, pp. 223–228. IEEE, 2016.

O'shea, T. and Hoydis, J. An introduction to deep learning for the physical layer. *IEEE Transactions on Cognitive Communications and Networking*, 3(4):563–575, 2017.

Pentina, A., Sharmanska, V., and Lampert, C. H. Curriculum learning of multiple tasks. In *Proceedings of the IEEE Conference on Computer Vision and Pattern Recognition*, pp. 5492–5500, 2015.

Platanios, E. A., Stretcu, O., Neubig, G., Poczos, B., and Mitchell, T. M. Competence-based curriculum learning for neural machine translation. *arXiv preprint arXiv:1903.09848*, 2019.

Plotkin, M. Binary codes with specified minimum distance. *IRE Transactions on Information Theory*, 6(4):445–450, 1960.

Polyanskiy, Y., Poor, H. V., and Verdú, S. Channel coding rate in the finite blocklength regime. *IEEE Transactions on Information Theory*, 56(5):2307–2359, 2010.

Qin, Z., Ye, H., Li, G. Y., and Juang, B.-H. F. Deep learning in physical layer communications. *IEEE Wireless Communications*, 26(2):93–99, 2019.

Radford, A., Wu, J., Child, R., Luan, D., Amodei, D., Sutskever, I., et al. Language models are unsupervised multitask learners. *OpenAI blog*, 1(8):9, 2019.

Reed, S. and De Freitas, N. Neural programmer-interpreters. *arXiv preprint arXiv:1511.06279*, 2015.

Richardson, T. and Urbanke, R. *Modern coding theory*. Cambridge University Press, 2008.

Rowshan, M. and Viterbo, E. On convolutional precoding in pac codes. In *2021 IEEE Globecom Workshops (GC Wkshps)*, pp. 1–6. IEEE, 2021a.

Rowshan, M. and Viterbo, E. List viterbi decoding of pac codes. *IEEE Transactions on Vehicular Technology*, 70(3):2428–2435, 2021b.

Rowshan, M., Burg, A., and Viterbo, E. Complexity-efficient fano decoding of polarization-adjusted convolutional (pac) codes. In *2020 International Symposium on Information Theory and Its Applications (ISITA)*, pp. 200–204. IEEE, 2020a.

Rowshan, M., Burg, A., and Viterbo, E. Polarization-adjusted convolutional (pac) codes: Fano decoding vs list decoding. *arXiv preprint arXiv:2002.06805*, 2020b.

Sanh, V., Debut, L., Chaumond, J., and Wolf, T. Distilbert, a distilled version of bert: smaller, faster, cheaper and lighter, 2019. URL https://arxiv.org/abs/1910.01108.

Shannon, C. E. A mathematical theory of communication. *The Bell system technical journal*, 27(3):379–423, 1948.

Sun, H., Viterbo, E., and Liu, R. Optimized rate-profiling for pac codes. *arXiv preprint arXiv:2106.04074*, 2021.

Tal, I. and Vardy, A. How to construct polar codes. *IEEE Trans. Inf. Theory*, 59(10):6562–6582, 2013.

Tal, I. and Vardy, A. List decoding of polar codes. *IEEE Transactions on Information Theory*, 61(5):2213–2226, 2015.

Trifonov, P. A score function for sequential decoding of polar codes. In *2018 IEEE International Symposium on Information Theory (ISIT)*, pp. 1470–1474, 2018. doi: 10.1109/ISIT.2018.8437559.

Vasić, B., Xiao, X., and Lin, S. Learning to decode ldpc codes with finite-alphabet message passing. In *2018 Information Theory and Applications Workshop (ITA)*, pp. 1–9. IEEE, 2018.

Vaswani, A., Shazeer, N., Parmar, N., Uszkoreit, J., Jones, L., Gomez, A. N., Kaiser, Ł., and Polosukhin, I. Attention is all you need. In *Advances in Neural Information Processing Systems*, pp. 5998–6008, 2017.

Wang, X., Chen, Y., and Zhu, W. A survey on curriculum learning. *IEEE Transactions on Pattern Analysis and Machine Intelligence*, 2021.

Wang, Y., Perazzi, F., McWilliams, B., Sorkine-Hornung, A., Sorkine-Hornung, O., and Schroers, C. A fully progressive approach to single-image super-resolution. In *Proceedings of the IEEE conference on computer vision and pattern recognition workshops*, pp. 864–873, 2018.

Wang, Y., Gan, W., Yang, J., Wu, W., and Yan, J. Dynamic curriculum learning for imbalanced data classification. In *Proceedings of the IEEE/CVF International Conference on Computer Vision*, pp. 5017–5026, 2019.

Wang, Z., Wohlwend, J., and Lei, T. Structured pruning of large language models. In *Proceedings of the 2020 Conference on Empirical Methods in Natural Language Processing (EMNLP)*. Association for Computational Linguistics, 2020. doi: 10.18653/v1/2020.emnlp-main. 496. URL https://doi.org/10.18653%2Fv1%2F2020.emnlp-main.496.

Wu, X., Dyer, E., and Neyshabur, B. When do curricula work? *arXiv preprint arXiv:2012.03107*, 2020.

Xu, W., You, X., Zhang, C., and Be'ery, Y. Polar decoding on sparse graphs with deep learning. In *2018 52nd Asilomar Conference on Signals, Systems, and Computers*, pp. 599–603. IEEE, 2018.

Yao, H., Fazeli, A., and Vardy, A. List decoding of arıkan's pac codes. *Entropy*, 23(7):841, 2021.

Yuan, B. and Parhi, K. K. Early stopping criteria for energy-efficient low-latency belief-propagation polar code decoders. *IEEE transactions on signal processing*, 62(24): 6496–6506, 2014.

Zaremba, W. and Sutskever, I. Learning to execute. *arXiv preprint arXiv:1410.4615*, 2014.

Zhu, H., Cao, Z., Zhao, Y., Li, D., and Yang, Y. Fast list decoders for polarization-adjusted convolutional (pac) codes. *arXiv preprint arXiv:2012.09425*, 2020.

A. Successive Cancellation decoder

Here we detail the successive-cancellation (SC) algorithm for decoding polar codes. As a motivating example, let's consider the Polar$(2, 2)$ code. Let the two information bits be denoted by u and v, where $u, v \in \{0, 1\}$. The codeword $x \in \{0, 1\}^2$ is given by $x = (x_1, x_2) = (u \oplus v, v)$. Let $y \in \mathbb{R}^2$ be the corresponding noisy codeword received by the decoder. First we convert the received y into a vector of log-likelihood-ratios (LLRs), $L_y \in \mathbb{R}^2$, which contains the soft-information about coded bits x_1 and x_2, i.e.

$$
\begin{aligned}
L_y &= (L_y^{(1)}, L_y^{(2)}) \\
&\triangleq \left(\log \frac{\mathbb{P}[y_1|x_1 = 0]}{\mathbb{P}[y_1|x_1 = 1]}, \log \frac{\mathbb{P}[y_2|x_2 = 0]}{\mathbb{P}[y_2|x_2 = 1]} \right) \in \mathbb{R}^2.
\end{aligned}
$$

Once we have the soft-information about the codeword x, the goal is to now obtain the same for the message bits u and v. To compute the LLRs for these information bits, SC uses the following principle: first, compute the soft-information for the left bit u to estimate $\hat{u}$. Use the decoded $\hat{u}$ to compute the soft-information for the right bit v and decode it. More concretely, we compute the LLR for the bit u as:

$$
L_u = \text{LSE}(L_y^{(1)}, L_y^{(2)}) = \log \frac{1 + e^{L_y^{(1)} + L_y^{(2)}}}{e^{L_y^{(1)}} + e^{L_y^{(2)}}} \in \mathbb{R}, \quad (6)
$$

where $\text{LSE}(a, b) \triangleq \log(1 + e^{a+b})/(e^a + e^b)$ for $a, b \in \mathbb{R}$. The expression in Eq. 6 follows from the fact that $u = (u \oplus v) \oplus v = x_1 \oplus x_2$ and hence the soft-information L_u can be accordingly derived from that of x_1 and x_2, i.e. L_y. Now we estimate the bit as $\hat{u} = \mathbb{1}\{L_u < 0\}$. Assuming that we know the bit $u = \hat{u}$, we observe that the codeword $x = (\hat{u} \oplus v, v)$ can be viewed as a two-repitition of v. Hence its LLR L_v is given by

$$
L_v = L_y^{(1)} \cdot (-1)^{\hat{u}} + L_y^{(2)} \in \mathbb{R}. \quad (7)
$$

Finally we decode the bit as $\hat{v} = \mathbb{1}\{L_v < 0\}$. To summarize, given the LLR vector L_y we first compute the LLR for the bit u, L_u, using Eq. 6 and decode it. Utilizing the decoded version $\hat{u}$, we compute the LLR L_v according to Eq. 7 and decode it.

For a more generic Polar(n, k), the underlying principle is the same: to decode a polar codeword $x = (u \oplus v, v)$, first decode the left child u and utilize this to decode the right child v. This principle is recursively applied at each node of the Plotkin tree until we reach the leaves of the tree where the decoding is trivial. In view of this principle, the SC algorithm for Polar$(2, 4)$, illustrated in Fig. 3(b), can be

mathematically expressed as (in the sequence of steps):

$$
\begin{aligned}
y &\in \mathbb{R}^4 \\
L_y &= (L_y^{(1)}, L_y^{(2)}, L_y^{(3)}, L_y^{(4)}) \in \mathbb{R}^4, \\
L_u &= (\text{LSE}(L_y^{(1)}, L_y^{(3)}), \text{LSE}(L_y^{(2)}, L_y^{(4)})) \in \mathbb{R}^2,
\end{aligned}
$$

frozen $\longrightarrow \hat{m}_1 = 0,$

$$
\begin{aligned}
L_2 &= \text{LSE}(L_y^{(1)}, L_y^{(3)}) + \text{LSE}(L_y^{(2)}, L_y^{(4)}) \in \mathbb{R}, \\
\hat{m}_2 &= \mathbb{1}\{L_2 < 0\} \in \{0, 1\}, \\
\hat{u} &= (\hat{m}_2, \hat{m}_2) \in \{0, 1\}^2, \\
L_v &= (L_y^{(1)}, L_y^{(2)}) \cdot (-1)^{\hat{u}} + (L_y^{(3)}, L_y^{(4)}) \in \mathbb{R}^2,
\end{aligned}
$$

frozen $\longrightarrow \hat{m}_3 = 0,$

$$
\begin{aligned}
L_4 &= L_v^{(1)} + L_v^{(2)} \in \mathbb{R}, \\
\hat{m}_4 &= \mathbb{1}\{L_4 < 0\} \in \{0, 1\}.
\end{aligned}
$$

In Fig. 3(b), the above equations are succinctly represented by two set of arrows: the black solid arrows represent the flow of soft-information from the parent node to the children whereas the green dotted arrows represent the flow of the decoded bit information from the children to the parent. We note that we use a simpler min-sum approximation for the function LSE that is often used in practice, i.e.
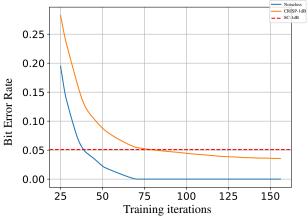
$$
\text{LSE}(a, b) \approx \min(|a|, |b|)\text{sign}(a)\text{sign}(b), \quad a, b \in \mathbb{R}.
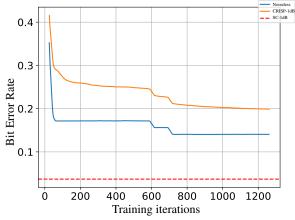$$

B. Interpretation

As discussed in Sec. 4.4, we observe that whenever our decoder reaches SC or better performance eventually when training at a specific SNR, its BER (over all the bits) on uncorrupted codewords, noiseless BER, drops to 0 early on in the training. Fig. 7(a) illustrates this for Polar$(32, 16)$. Conversely, if the model gets stuck at a BER worse than that of SC, then we observe that its noiseless BER is also stuck at a non-zero value. This is highlighted in Fig. 7(b) for Polar$(64, 32)$. In particular, we notice that the least reliable bits contribute the most to the noiseless BER, while a majority of the cleaner bits have zero individual BER (Fig. 8(a)). Viewed from this context, we focus on the noiseless scenario, i.e. $y = x$.

As a motivating example, we first consider the Polar$(4, 4)$ code. Let $m = (m_1, m_2, m_3, m_4) \in \{0, 1\}^4$ be the block of message bits and $x \in \{0, 1\}^4$ be the codeword. Hence under the L2R curriculum, the subcodes evolve as

- $k = 1 : m_1 \mapsto (m_1, 0, 0, 0) \mapsto x = (m_1, 0, 0, 0),$

- $k = 2 : (m_1, m_2) \mapsto (m_1, m_2, 0, 0) \mapsto x = (m_1 \oplus m_2, m_2, 0, 0),$

- $k = 3 : (m_1, m_2, m_3) \mapsto (m_1, m_2, m_3, 0) \mapsto x = (m_1 \oplus m_2 \oplus m_3, m_2, m_3, 0),$

(a) Noiseless BER goes to zero when the model is better than SC

(b) Noiseless BER is high when the model is worse than SC

Figure 7: Evolution of training BER at 1dB and noiseless BER for CRISP.

- $k = 4 : (m_1, m_2, m_3, m_4) \mapsto (m_1, m_2, m_3, m_4) \mapsto$
  $\boldsymbol{x} = (m_1 \oplus m_2 \oplus m_3 \oplus m_4, m_2 \oplus m_4, m_3 \oplus m_4, m_4)$.

Correspondingly, their optimal bit decoding rules under the MAP evolve as

- $k = 1 : \boldsymbol{y} = \boldsymbol{x} = (m_1, 0, 0, 0) \mapsto \hat{m}_1 = x_1$,

- $k = 2 : \boldsymbol{y} = \boldsymbol{x} = (m_1 \oplus m_2, m_2, 0, 0) \mapsto (\hat{m}_1, \hat{m}_2) = (x_1 \oplus x_2, x_2)$,

- $k = 3 : \boldsymbol{y} = \boldsymbol{x} = (m_1 \oplus m_2 \oplus m_3, m_2, m_3, 0) \mapsto (\hat{m}_1, \hat{m}_2, \hat{m}_3) = (x_1 \oplus x_2 \oplus x_3, x_2, x_3)$,

- $k = 4 : \boldsymbol{y} = \boldsymbol{x} = (m_1 \oplus m_2 \oplus m_3 \oplus m_4, m_2 \oplus m_4, m_3 \oplus m_4, m_4) \mapsto (\hat{m}_1, \hat{m}_2, \hat{m}_3, \hat{m}_4) = (x_1 \oplus x_2 \oplus x_3 \oplus x_4, x_2 \oplus x_4, x_3 \oplus x_4, x_4)$.

Similarly, we can compute the subcodes and their corresponding decision rules under the R2L curriculum. Fig. 9 illustrates this evolution for both L2R and R2L. For the least reliable bit m_1, we observe that the L2R curriculum reaches the optimal rule more gracefully by including one coordinate x_i at a time while this change for R2L (and no-curriculum) is abrupt, making it harder to learn. We observe the same trend for other bits m_2, m_3 and m_4. Note that for Polar$(4, 4)$, the reliability order is $m_1 < m_2 = m_3 < m_4$ and hence the L2R curriculum is same as N2C and R2L is same as C2N.

For a general Polar(n, k), we can likewise compute the optimal MAP rules using the fact that the mapping PlotkinTree : $\{0, 1\}^n \to \{0, 1\}^n$ is its own inverse, i.e. $\boldsymbol{x} = \text{PlotkinTree}(\boldsymbol{m}) \implies \boldsymbol{m} = \text{PlotkinTree}(\boldsymbol{x})$.

To concretely compare different curricula, we define the notion of *learning difficulty* for a bit: the number of codeword bits multiplied in its optimal decoding rule. This metric roughly captures the number of multiplication operations a model has to learn at any curriculum step. For example, for Polar$(4, 4)$, the learning difficulty for m_1 evolves as $1 \to 2 \to 3 \to 4$ for the L2R curriculum and as $0 \to 0 \to 0 \to 4$ for the R2L curriculum. Fig. 10 illustrates the evolution of learning difficulty (taking maximum over all bits) for Polar$(32, 16)$ and Polar$(64, 22)$ codes. We observe here that the jumps in the learning difficulty are larger for R2L, thus indicating a harder transfer than L2R, where it increases smoothly (at most one bit per step).

Fig. 12 highlights a similar phenomenon for Polar$(64, 22)$ for L2R, R2L, N2C and C2N curricula. We observe that the learning difficulties of the L2R and N2C curricula evolve smoothly while that of R2L and C2N are abrupt. Correspondingly, their final BER reliability performance follows the order N2C $\approx$ L2R < R2L $\approx$ C2N (Fig. 11).

B.1. Error analysis

To interpret the CRISP decoder, we compare its bitwise error patterns against the SCL decoder. As shown in Fig. 8(b), we plot the contribution of each bit to the block error rate; we condition on having no previous errors. We observe that the typical error events of CRISP, unlike CRISP_CNN, closely resemble that of the SCL decoder. This aligns with our expectation since CRISP uses a sequential decoding paradigm similar to that of the successive cancellation framework.

(a) Bitwise BER for clean and noisy bits

(b) Bitwise contribution to the total BLER

Figure 8: Error analysis for Polar$(64, 22)$: (a) Noiseless BER for the two least reliable bits gets stuck at 0.5 whereas it converges to 0 for the two most reliable bits, (b) Contribution of each bit (conditioned on no previous errors) to the BLER.
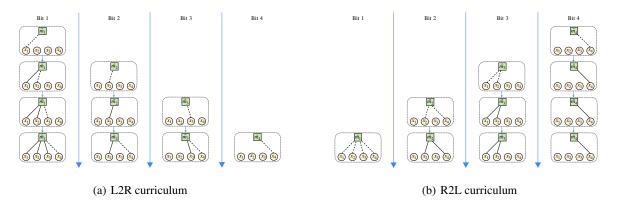

(a) L2R curriculum

(b) R2L curriculum

Figure 9: Evolution of the MAP decoding rules for L2R and R2L for Polar$(4, 4)$. Dotted lines indicate new coded bits being introduced into the decoding rule at each curriculum step.

C. Ablation studies

Recall that our CRISP decoder consists of the sequential RNN (512-dim hidden state) trained with the L2R curriculum. To understand the contribution of each of these components to its gains over SC, we did the following ablation experiments for Polar$(64, 22)$ code.

C.1. Effect of model size

We fix the decoder to be GRU and consider different model sizes via the hidden state size $h \in \{256, 512\}$, and different curricula among {L2R, R2L, Without curriculum (w/o C)}. Fig. 13(a) demonstrates that the accuracy gains of the L2R curriculum are more pronounced for *smaller* models ($h = 256$). On the other hand, we observe minimal reliabilty gains for L2R with large models ($h = 512$). We also tried

other sequential architectures such as LSTMs (Hochreiter & Schmidhuber, 1997) and Transformers (Radford et al., 2019), but found GRUs to be the best (App. D).

C.2. Sequential vs. block decoding

The sequential GRU architecture for CRISP is inspired in part by the sequential SC algorithm. Alternatively, we also design CRISP_CNN, a block decoder parameterized by 1D Convolutional Neural Networks (CNNs). CRISP_CNN estimates all the information bits m_i in one shot given $\boldsymbol{y}$. Similar to sequential decoders, curriculum learning; in particular, the L2R scheme works the best for block decoding in achieving near-MAP reliability.

Fig. 14(b) compares RNNs and CNNs in terms of BLER for Polar$(64, 22)$ with L2R and R2L curricula. We observe

(a) Polar(32, 16)

(b) Polar(64, 22)

Figure 10: Evolution of the learning difficulty for L2R and R2L.

(a) Polar(32, 16)

(b) Polar(64, 22)

Figure 11: Choice of curriculum is crucial to obtain gains over SC. Information-theory guided curricula N2C and C2N are marginally better than the L2R and R2L schemes respectively.

that RNN-based decoders (CRISP) are more reliable in terms of BLER than CNNs; in contrast, RNNs and CNNs achieve similar BER performance (Fig. 14(a)). Further, we observe that the error patterns corresponding to bitwise contribution to the total BLER for the RNN model resemble that of SC-List, as opposed to CNN models (Fig. 8(b)). We show the evolution of validation BER for CNN training in Fig. 15(a). We see that the C2N curriculum performs worse than the N2C curriculum.

D. Additional results

We present our additional results on the Polar code family with various decoding architectures such as CNNs and transformers, with BLER reliability, and for longer blocklengths ($n = 128$). Recall that the CRISP decoder uses the GRU-based RNN (Fig. 4(a)) trained with the L2R curriculum.

D.1. Additional results for polar codes

D.1.1. ROBUSTNESS TO NON-AWGN NOISE

In this section we evaluate CRISP trained on AWGN on non-AWGN settings. We test CRISP on a Rayleigh fading channel, and T-distributed noise. As shown in Fig. 16, CRISP retains its gains when tested on a Rayleigh fading channel. Further, as demonstrated in Fig. 17, CRISP is very robust to T-distributed noise and marginally outperforms SCL at higher SNRs. These experiments suggest that the CRISP decoder inherits the robustness inherent to nearest neighbor decoding even though this was not explicitly featured in the training – this intuition is further justified by our experiments showing that the typical error events of CRISP match that of the optimal SCL (MAP) decoder (App. B.1)

D.1.2. GENERALIZATION TO UNSEEN CODEWORDS

We emphasize that the CRISP decoder does not rely on memorizing codewords to achieve its high performance. We
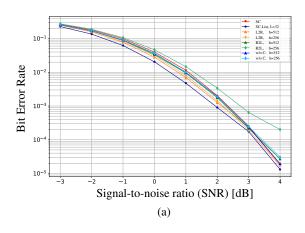
(a) Noisiest bit

(b) Maximum over all bits

Figure 12: Evolution of learning bit difficulty for different curricula for Polar$(64, 22)$.
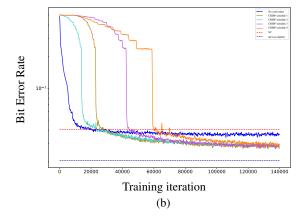

(a)

(b)

Figure 13: Ablation plots: (a) Choosing the right curriculum is critical when model size is smaller, (b) The number of iterations to train CRISP on each subcode using the L2R/N2C curriculum are not critical to the final performance achieved.

demonstrate this on a Polar$(64, 22)$ codebook consisting of 2^22 codewords, where we randomly selected subsets comprising of the codebook as training data, and held out the remaining codewords for evaluation. We observe in Fig. 15(b) that the CRISP decoder trained on a limited set of codewords does not lead to performance deterioration. This shows that our training method learns the structural patterns inherent to Polar and PAC codes, rather than just memorizing the codewords.

D.1.3. CRISP FOR CRC-POLAR CODES

In practice, polar codes with successive cancellation list decoding is used in conjunction with a cyclic redundancy check (CRC) outer code. The message $u \in \{0, 1\}^{k_m}$ is encoded by a systematic cyclic code of rate $\frac{k_m}{k}$ to obtain a vector $m \in \{0, 1\}^k$. We obtain the codewords via the normal polar encoding procedure on m. CRISP can be used to decode such CRC-Polar codes by considering m as the input to the polar code block. As shown in Fig. 18, CRISP

achieves near-MAP reliability when CRCs of length 3 and 8 are used for a Polar$(64, 22)$ code.

D.1.4. SCALING TO LARGER CODES

Curriculum training can be used to train even larger codes and obtain gains over naive training methods. However, we observed that our models were only able to achieve a reliability marginally better than SC. As shown in Fig. 21, CRISP performs similar to SC decoding on the Polar$(128, 22)$ code. We believe that it is possible to close the gap with MAP with more training tricks.

D.1.5. RESULTS WITH TRANSFORMERS

We also experimented with transformer-based architecures (Vaswani et al., 2017) for our decoder. In particular, we tried an autoregressive transformer-decoder network (similar to GPT (Brown et al., 2020) that does sequential decoding) and the transformer-encoder network (similar to BERT (Devlin et al., 2018) that does block decoding). Preliminary
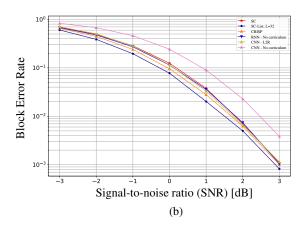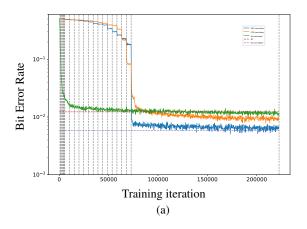
Figure 14: a) CNN decoder achieves near-MAP BER performance with L2R curriculum.
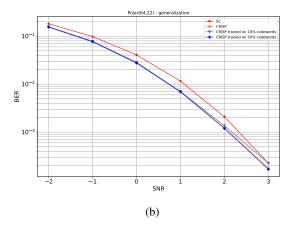b) CRISP achieves near-MAP BLER for Polar$(64, 22)$. CNN is slightly worse.

Figure 15: (a) L2R curriculum helps CNN to achieve near-optimal reliability

results indicate that these transformer-based models are less reliable compared to RNNs and CNNs (Fig. 19). In addition, these models take a greater number of iterations (E) to train on each of the subcodes than RNNs and CNNs during curriculum training. Transformer training is sensitive to architectural and hyperparameter choices and is computationally expensive. We believe that with the right training tricks, transformer-based models can be used to decode larger codes. This is ongoing work.

D.2. Additional results for PAC codes

CRISP maintains its good performance even in block error rate, as we show in Fig. 20(b). Fig. 20(a) compares RNNs and CNNs in terms of BER for PAC$(32, 16)$ code with L2R and R2L curricula. We observe that while both RNNs and CNNs outperform SC, RNNs achieve slightly better

BER reliability than CNNs. On the other hand, Fig. 20(b) highlights that CNNs achieves an SC-like BLER.

E. Experimental details

We provide our code at the following link.

Data generation. Note that for any Polar(n, k) or PAC(n, k) code, the input message m is chosen uniformly at random from $\{0, 1\}^k$. We simulate this by drawing k i.i.d. Bernoulli random variables with probability $1/2$. We follow a similar procedure to generate a batch of message blocks (in $\{0, 1\}^{B \times k}$) with batch size B, both during training and inference. For the AWGN channel, the batch noise (in $\mathbb{R}^{B \times n}$) is accordingly generated by drawing i.i.d. Gaussian samples from $\mathcal{N}(0, \sigma^2)$.
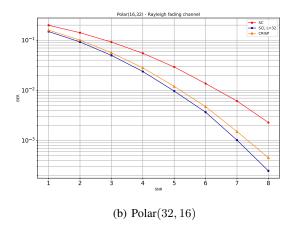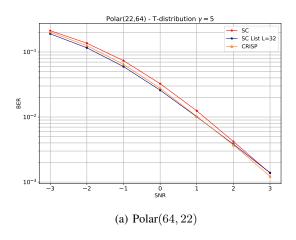
(a) Polar(64, 22)

(b) Polar(32, 16)

Figure 16: CRISP achieves good reliability on Rayleigh fading channels
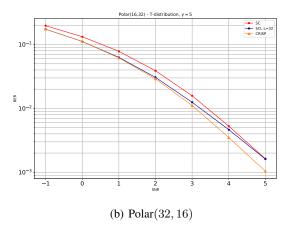

(a) Polar(64, 22)

(b) Polar(32, 16)

Figure 17: CRISP matches SCL reliability on T-distributed channels

Hyper-parameters. For training our models (both sequential and block decoders), we use AdamW optimizer (Loshchilov & Hutter, 2017) with a learning rate of 10^{-3}. At each curriculum step, corresponding to training a sub-code, we choose the SNR corresponding to which the optimal decoder for that subcode has BER in the range of $10^{-2} \sim 10^{-1}$ (Kim et al., 2018b). This ensures that a significant portion of training examples lie close to the decision boundary. It is well known that using a large batch size is essential to train a reliable decoder (Jiang et al., 2019a); we use a batch size of 4096 or 8192.

E.1. Sequential decoders

We present the architectures and training details for our sequential decoders. We consider two popular choices for our sequential models: RNNs and GPT. We also note that it is a standard practice to use *teacher forcing* to train sequential

models (Lamb et al., 2016): during training, as opposed to feeding the model prediction $\hat{m}_i$ as an input for the next time step, the ground truth message bit m_i is provided as an input to the model instead (Fig. 4(a)). *Student forcing* refers to using the same $\hat{m}_i$ as an input.

E.1.1. RNNs

Architecture. We use a 2-layer GRU with a hidden state size of 512. The output at each timestep is obtained through a fully connected layer (as shown in Fig. 4(a)). The network has 2.5M and 600K parameters for block lengths 64 and 32. As shown in Figure 22, 2-layer-LSTM and 3-layer-GRU models achieve similar performance. We choose a 2-layer GRU for our experiments since it allows for faster training and has fewer parameters.
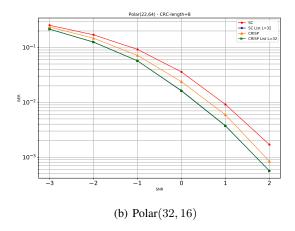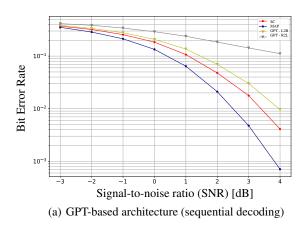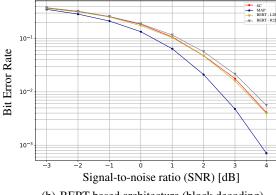
(a) Polar(64, 22)

(b) Polar(32, 16)

Figure 18: CRISP performs well on CRC-Polar code

(a) GPT-based architecture (sequential decoding)
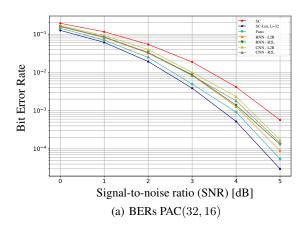

(b) BERT-based architecture (block decoding)

Figure 19: Transformer performance on Polar(32, 16).

Training. We use the teacher forcing mechanism to train our models. We found that teacher forcing gives a better final performance in terms of both BER and BLER, whereas student forcing only provides gains in the BER reliability (Fig. 23). We observed that student forced training achieved sub-optimal performance for larger block lengths. Empirically we observed that the number of iterations spent on training each intermediate subcode of the curriculum is not critical to the performance of the final model (Fig. 13(b)). To train CRISP for Polar(64,22), we use the following curriculum schedule: Train each subcode for 2000 iterations, and finally train the full code until convergence with a decaying learning rate. This training schedule required 13-15 hours of training on a GTX 1080Ti GPU.

E.1.2. GPT

Architecture. The model consists of 6 transformer blocks with masked self-attention and GELU activation. The multiheaded attention unit has 8 heads in each block, and an embedding/hidden size of 64 is used throughout the network. The output vectors of the final transformer block are passed through a linear layer to estimate each bit sequentially. The model has 350K parameters for blocklength 32.

Training. For training the GPT-based transformer, we use a teacher forcing mechanism. Here, we observed that the decoder takes a greater number of iterations ($40,000$) to train on each of the subcodes than RNNs and CNNs ($2,000 - 10,000$) during curriculum training of Polar(32, 16). For a fixed batch size, GPT also takes significantly longer to train (12 hours) compared to CNNs (3 hours) and RNNs (4 hours) on GTX 1080 Ti GPU.
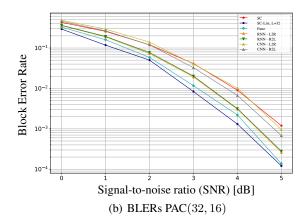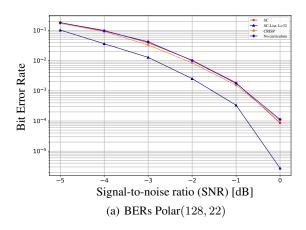
(a) BERs PAC$(32, 16)$

(b) BLERs PAC$(32, 16)$

Figure 20: With correct choice of curriculum, CNNs match the BER performance of CRISP on PAC(32,16). However, they are sub-optimal in BLER.
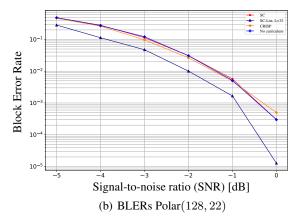

(a) BERs Polar$(128, 22)$

(b) BLERs Polar$(128, 22)$

Figure 21: CRISP matches SC reliabilty on Polar$(128, 22)$.

E.2. Block decoders

E.2.1. CNNs

Architecture. For block decoding using Convolutional Neural Networks (CNNs), we use a ResNet-like architecture (He et al., 2015), with the primary difference being the use of 1D convolutions instead of 2D. The model has 10 1D-convolutional layers with residual connections skipping every two consecutive layers. Each convolutional layer has 64 channels, which are flattened at the penultimate layer and fed as an input to a fully-connected neural network with one hidden layer. We use the GELU (Hendrycks & Gimpel, 2016) activation function throughout the network. The model has 2.5M parameters for blocklength 64.
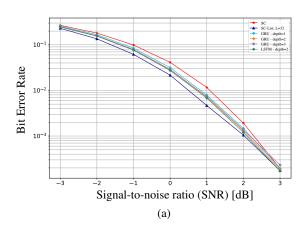
Training. We train the CNN model for $5,000$ iterations for each intermediate subcode of the curriculum. In the last step

of the curriculum, we train it for $100,000$ iterations with a decaying cosine annealing schedule for the learning rate (Loshchilov & Hutter, 2016).

E.2.2. BERT

Architecture. The model consists of 6 transformer blocks with unmasked self-attention and GELU activation. In each block, the multiheaded attention unit has 8 heads, and an embedding/hidden size of 64 is used throughout the network. The output vectors of the final transformer block are passed through a linear layer to estimate all the bits in one shot. The model has 350K parameters for blocklength 32.

Training. We train this model on each intermediate subcode for around $10,000 - 20,000$ steps. Thus the BERT-based decoder achieves better reliability than its GPT counterpart
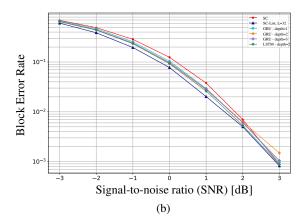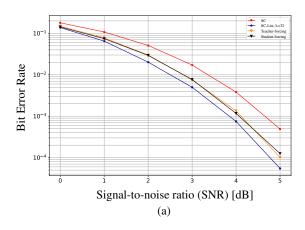
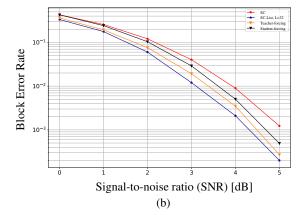Figure 22: Polar(64, 22): LSTMs and GRUs achieve similar reliability.

Figure 23: Training CRISP using student forcing results in sub-optimal BLER.

despite fewer training iterations (Fig. 19).

F. Reliability-complexity comparison

Two important metrics in evaluating a decoding algorithm are the decoding reliability and complexity. In this paper, we focus on optimizing the BER performance; the main goal of our paper is to design a curriculum based decoder for Polar and PAC codes that can achieve near-optimal reliability performance as opposed to the current data-driven approaches that only match the SC. In Sec. 4.2, we demonstrated that CRISP achieves excellent inference throughput on GPUs. We also see that the decoding complexity of CRISP can be further improved with a hardware-aware neural architecture.

We believe that neural decoders, coupled with the recent advances in distillation (Sanh et al., 2019) and pruning of neural networks (Hinton et al., 2015; Wang et al., 2020; An-

war et al., 2015) far larger than ours (E.g., 110M for BERT vs. 2.5M for CRISP), can achieve even better runtimes. For instance, TinyBERT ((Jiao et al., 2019)) uses knowledge distillation to learn a model 9.4x faster on inference compared to the parent BERT. Coupled with efficient GPU implementations, which are optimized for vector-matrix multiplications, and the aforementioned compression techniques, we believe neural decoders offer a great potential for fast and reliable channel decoding. It is important to note that inference throughput is hardware and software dependant. In Table 1, we report throughput numbers of the optimized C++ multithreaded implementation of SC/SCL decoding on CPU using the aff3ct toolbox ((Cassagne et al., 2019)). There has been progress in developing GPU implementations of SCL ((Cammerer et al., 2017b; Han et al., 2017)). Since we could not find publicly available implementations of these works, we report throughput numbers of our implementation.